Multiscale integration of environmental stimuli in plant tropism produces complex behaviors

Derek E. Moulton[1], **Hadrien Oliveri, and Alain Goriely**[1]

Mathematical Institute, University of Oxford, Oxford OX2 6GG, United Kingdom

This manuscript was compiled on November 7, 2020

Plant tropism refers to the directed movement of an organ or organism in response to external stimuli. Typically, these stimuli induce hormone transport that triggers cell growth or deformation. In turn, these local cellular changes create mechanical forces on the plant tissue that are balanced by an overall deformation of the organ, hence changing its orientation with respect to the stimuli. This complex feedback mechanism takes place in a three-dimensional growing plant with varying stimuli depending on the environment. We model this multiscale process in filamentary organs for an arbitrary stimulus by linking explicitly hormone transport to local tissue deformation leading to the generation of mechanical forces and the deformation of the organ in three dimensions. We show, as examples, that the gravitropic, phototropic, nutational, and thigmotropic dynamic responses can be easily captured by this framework. Further, the integration of evolving stimuli and/or multiple contradictory stimuli can lead to complex behavior such as sun following, canopy escape, and plant twining.

Plant tropism | Biomechanics | Morphoelasticity | Rod theory | Mathematical model

Plant tropism is the general phenomenon of directed growth and deformation in response to stimuli. It includes phototropism, a reaction to light (1); gravitropism, the reaction to gravity (2, 3); and thigmotropism, a response to contact (4), among many others (see Fig. 1). The study of tropisms in plants dates back to the pioneering work of giants such as Darwin (5) and Sachs (6), and has been a central topic for our understanding of plant physiology ever since. Tropisms form a cornerstone subject of modern plant biomechanics (7), crop management strategies (8), as well as systems biology and plant genomics (9). Being sessile by nature, plants lack the option to migrate and must adapt to their ever-changing environment. The growth response of individual plants to environmental cues will determine the yield of a crop in unusually windy conditions, will decide the future of rainforests in a world driven by climate change, and may be key for colonizing foreign environments such as Mars.

Mathematical modeling plays an invaluable role in gaining a better understanding of tropisms and how plants may respond to a change in their environment (10). Yet, a general mathematical description of tropisms is a grand challenge. First, the growth response tends to be dynamically varying: a sunflower grows to face the sun, but as it grows the sun moves, so the environmental influence – the intensity of light impacting on each side of the sunflower – is changing during the process. Similarly, a tree branch may align with the vertical in a gravitropic response; decreasing the likelihood of breaking under self-weight; however, the growth response itself may increase the branch weight and thus change the stimulus (11). Second, while there exist numerous experimental setups that enable to carefully isolate a particular stimulus, a plant typically receives multiple stimuli at the same time and in different locations (12). The resulting movement is an integration of multiple signals. Third, any tropism is fundamentally a multiscale phenomenon. Transduction of an environmental cue takes place from the organ to the cell and involves, ultimately, molecular processes. A hormonal response is induced, which leads to different cells expanding at different rates in response to the chemical and molecular signals. However, one cannot understand the change in shape of the plant and its position in relation to the direction of the environmental stimulus at this level. To assess the effectiveness of the growth response, one needs to zoom out. The net effect of a non-uniform cell expansion due to hormone signaling is a tissue-level differential growth (1) as depicted in Fig. 2. At the tissue level, each cross section of the plant can be viewed as a continuum of material that undergoes non-uniform growth and/or remodeling (17). Differential growth locally creates curvature and torsion, but it also generates residual stress (18). As a result, the global shape of the plant and its material properties evolve in time. To characterize this global change, and to update the position of the plant in the external field, a further zooming out to the plant or organ level is appropriate. At the plant level, the global shape, material properties, and positioning in the external stimulus are well described by a physical filament: here, the plant is viewed as a space curve endowed with physical properties dictated by the lower level tissue scale, and its shape and motion can be described by the theory of elastic rods, which has been applied to multiple biological contexts,

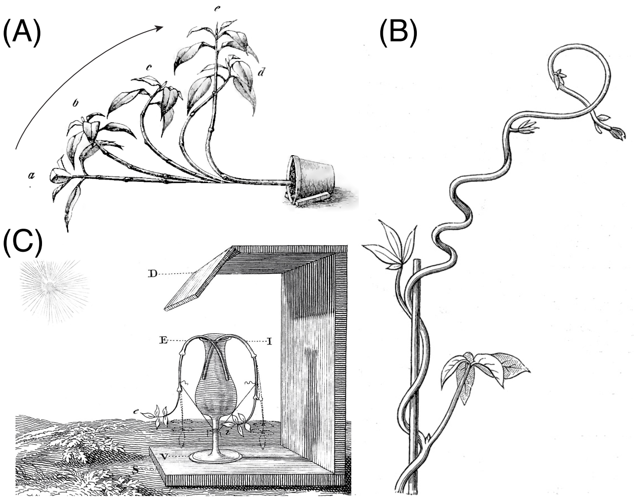

Fig. 1. Classic experiments on tropic responses. (A) Gravitropism: a potted plant realigns itself with gravity (13). (B) Thigmotropism: a twining vine develops curvature when in contact with a pole (6). (C) Phototropism: a plant reorients itself towards the light source (18th Century experiments by Bonnet (14), correctly interpreted by Duhamel du Monceau (15, 16)).

from DNA and proteins, to physiology and morphogenesis (19–22).

The challenge of formulating a mathematical model of tropism is further complicated by the remarkable variation in plants and the multiple types of tropism. Within a single plant, a tropic response may refer to the growth and movement of the entire plant, or a subset: a single branch, vine, stem, or root. Here, we use the word ‘plant’ to refer to the entire class of plant structures that may undergo such growth responses. Moreover, even within a single plant, multiple environmental cues will combine and overlap in effecting mechanotransductive signals, hormonal response, differential growth, and ultimate change in shape (23); e.g. a sunflower exhibiting phototropism still perceives a gravitational signal.

At the theoretical level, a variety of approaches have recently been proposed. Growth kinematics models successfully describe the tropic response at the plant level (7, 24, 25), but do not include mechanics and cellular activities. A number of large-deformation elastic rod descriptions of tropic plant growth have also been proposed (26–31); these involve a full mechanical description at the plant level, with phenomenological laws for the dynamic updating of intrinsic properties such as bending stiffness and curvature, and even branching and self-weight (32), but specific cell- and tissue-level mechanisms are not included. Multiscale formulations have also appeared, including Functional-Structural Plant Models (8, 33, 34) and hybrid models with vertex-based cell descriptions (35, 36). These computational approaches have the potential to incorporate effects across scales but are limited to small deformations compared to the ones observed in nature.

The goal of this paper is to provide a robust mathematical theory that links scales and can easily be adapted to simulate and analyze a large number of overlapping tropisms for a spectrum of plant types. Our mathematical and computational framework includes (*i*) large deformations with changes of curvature and torsion in three-dimensional space; (*ii*) internal and external mechanical effects such as internal stresses, self-weight, and contact; and (*iii*) tissue-level transport of growth hormone driven by environmental signals. By considering the integration of multiple conflicting signals, we also provide a view of a plant as a problem-solving control system that is actively responding to its environment.

Significance Statement

To survive and to thrive, plants rely on their ability to sense multiple environmental signals, such as gravity or light, and respond to them by growing and changing their shape. To do so, the signals must be transduced down to the cellular level to create the physical deformations leading to shape changes. We propose a multiscale theory of tropism that takes multiple stimuli and transforms them into auxin transport that drives tissue-level growth and remodeling, thus modifying the plant shape and position with respect to the stimuli. This feedback loop can be dynamically updated to understand the response to individual stimuli or the complex behavior generated by multiple stimuli such as canopy escape or pole wrapping for climbing plants.

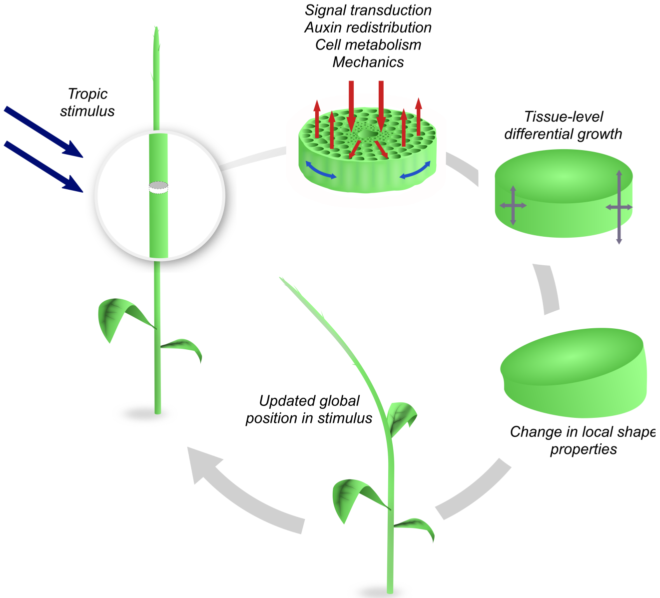

Fig. 2. Tropism is a multiscale dynamic process: the stimulus takes place at the plant or organ level and its information is transduced down to the cellular level creating a tissue response through shape inducing mechanical forces that change the shape of the organ. In the process, the plant reorients itself and, accordingly, the stimulus changes dynamically.

1. Multiscale modeling framework

The key to our multiscale approach is to join three different scales: stimulus-driven auxin transport at the cellular level; tissue-level growth mechanics; and organ-level rod mechanics.

A. Geometric description of the plant. We start at the organ scale and model the plant as a growing, inextensible, unshearable elastic rod following the formalism of (17, Chap. 5) that extends the classical Cosserat rod theory (37–40) to growing filaments. A *morphoelastic rod* is a one-dimensional filamentary object that can bend and twist with some penalty energy. The rod cannot be elastically stretched, but it can increase in length by addition of mass, leading to a *growth stretch*. Let $\mathbf{r}(S,t) \in \mathbb{R}^3$ describe its centerline, where S is the initial arc length measured from the base of the plant towards its tip (see Fig. 3(A)). Together with the fixed Cartesian basis, $\{\mathbf{e}_i;\ i=1,2,3\}$, we define, at each point on the curve $\mathbf{r}(S,t)$ a local orthonormal basis $\{\mathbf{d}_i;\ i=1,2,3\}$, oriented such that $\mathbf{d}_3$ aligns with the tangent $\partial\mathbf{r}/\partial S$ in the direction of increasing S, and $(\mathbf{d}_1,\mathbf{d}_2)$ denote directions in each cross section from the centerline to two distinguished material points. From the director basis, the Darboux vector is defined as $\mathbf{u} = \mathsf{u}_1\mathbf{d}_1 + \mathsf{u}_2\mathbf{d}_2 + \mathsf{u}_3\mathbf{d}_3$, and encodes the rod's curvature, torsion and twist (17). For a given curvature vector, the shape of the rod, and the evolution of the basis, is determined, for boundary conditions $\{\mathbf{r}(0),\mathbf{d}_1(0),\mathbf{d}_2(0),\mathbf{d}_3(0)\}$, by integrating the system of equations

$$\frac{\partial \mathbf{r}}{\partial S} = \gamma \mathbf{d}_3, \quad \frac{\partial \mathbf{d}_i}{\partial S} = \gamma \mathbf{u}\times\mathbf{d}_i, \quad i=1,2,3. \qquad [1]$$

All authors have contributed equally.

The authors declare no conflict of interest.

[1] To whom correspondence should be addressed. E-mail: moulton@maths.ox.ac.uk, goriely@maths.ox.ac.uk

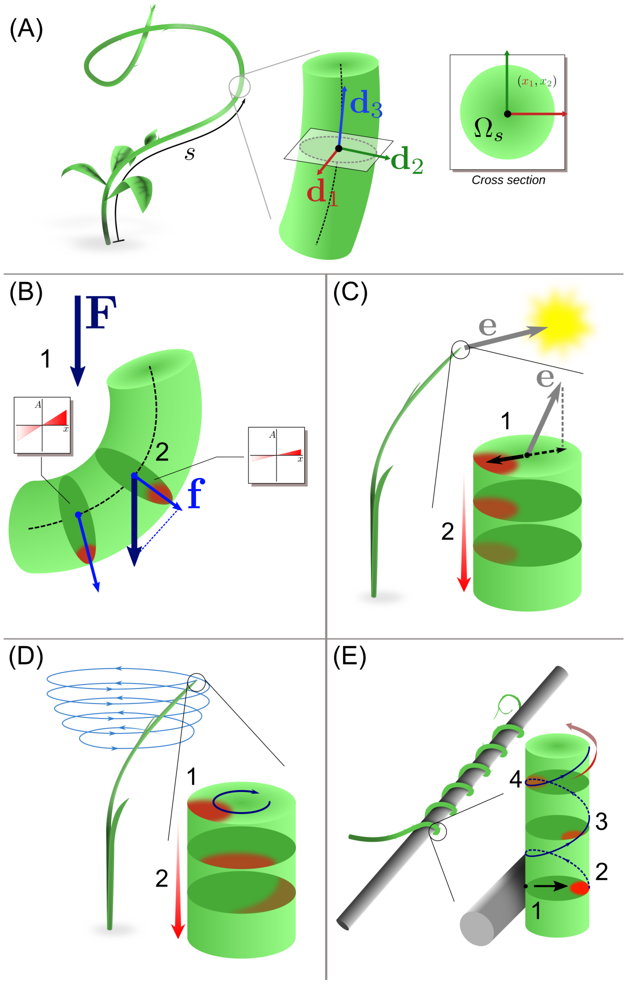

Fig. 3. (A) Each cross section Ω_s of the rod is parametrized by its arc length s (oriented acropetally) and equipped with a local material basis $\{\mathbf{d}_1, \mathbf{d}_2, \mathbf{d}_3\}$. (B) Gravitropism: the gravity vector (1) is sensed in each cross section and causes lateral auxin flow (2). (C) Phototropism: the light vector is sensed at the plant apex and results in the establishment of an apical auxin profile (1) that is transported basipetally with attenuation (2). (D) The circumnutation is generated by an internal oscillator with pulsation ω associated with rotating auxin profile at the apex (1). The apical profile is transported basipetally (2), generating curvature and torsion. (E) Thigmotropic pole wrapping is triggered by a contact (1) eliciting an asymmetrical auxin profile (2), which is in turn transported helically (3) to the rest of the plant with signal attenuation (4).

Here $\gamma := \partial s/\partial S$ denotes the total axial growth stretch of each section mapping the initial arc length S to the current arc length s (41). The general basis specializes to the Frenet-Serret frame by taking $\gamma = 1$ and $\mathbf{d}_1$ to be the curve's normal or to the so-called Bishop frame (or parallel transport frame) by taking $\gamma = 1$ and $\mathsf{u}_3 = 0$ (42, 43). At each value of S, the cross section is defined by a region $(x_1, x_2) \in \Omega_S \subset \mathbb{R}^2$, where x_1, x_2 are local variables describing the location of material points in the respective directions $\mathbf{d}_1$, $\mathbf{d}_2$. In terms of the local geometry, any material point $\mathbf{X} = X_1\mathbf{e}_1 + X_2\mathbf{e}_2 + X_3\mathbf{e}_3 \in \mathbb{R}^3$ in the plant can be represented by its arc length S and its position (x_1, x_2) on the cross section at S as follows:

$$\mathbf{X} = \mathbf{r}(S,t) + x_1\mathbf{d}_1(S,t) + x_2\mathbf{d}_2(S,t), \quad \text{for } (x_1, x_2) \in \Omega_S. \quad [2]$$

We can now use this representation to formulate the stimuli.

B. The stimuli. Tropic stimuli are characterized by their origin, sign, and direction (44). Signal *origin* includes: chemicals, water, humidity, gravity, temperature, magnetic fields, light, touch. Tropisms can have a *sign*: *positive* if the plant grows towards or in the direction of the stimulus or *negative* if it moves away from the stimulus. The *direction* of tropism describes the orientation of the response with respect to a directed stimuli: *exotropism* is the continuation of motion in the previously established direction, *orthotropism* is the motion in the same line of action as the stimulus, and *plagiotropism*, is the motion at an angle to a line of stimulus.

Physically, stimuli are fields acting in space at a point $\mathbf{X} \in \mathbb{R}^3$ and changing over time t. They can be either scalar fields, $f = f(\mathbf{X}, t)$, e.g. chemical, temperature, or light intensity; vector fields, $\mathbf{F} = \mathbf{F}(\mathbf{X}, t)$, e.g. geomagnetic field, gravity, or light direction; and, possibly, tensor fields (e.g. mechanical stress–not considered here). These stimuli are in general functions of both space and time which makes plant tropism a physical theory of fields (which is appropriate since plants grow in physical fields). Since a stimulus is defined at points in space, we must also take into account the orientation and the position of the plant in space. For example, the cellular response to light in phototropism is linked to the relative orientation of the plant in relation to the light source. In the case of a vector stimulus $\mathbf{F}$, we must therefore decompose the stimulus in the local basis:

$$\mathbf{F} = F_1\mathbf{d}_1 + F_2\mathbf{d}_2 + F_3\mathbf{d}_3, \quad F_i = \mathbf{F} \cdot \mathbf{d}_i, \quad i = 1, 2, 3. \quad [3]$$

The quantities (F_1, F_2, F_3) are the components of the stimulus as felt by the plant. Next, we link an external stimulus to the cellular response.

C. Cellular response and auxin transport. At the cellular level, deformations take place through anelastic expansions of the cell walls in response to turgor-induced tension (45, 46). We refer to any geometric change of cellular shape as growth. While detailed models of these cellular processes are available (47–49), they do not easily extend to the continuum level; hence, for simplicity we adopt here a coarse-grained view in which the anelastic expansions are connected locally via a single hormone concentration field that plays the role of a morphogen. This is in line with other models of morphogen-mediated growth (e.g. 50). Here, we consider the phytohormone *auxin* which is known to play a central role in plant growth and remodeling. Indeed, laterally asymmetrical auxin redistribution is broadly accepted as a universal mechanism underlying tropisms (51, 52). A lateral gradient is controlled via the relocalization of auxin transporters in response to tropic signals (53). In shoots, higher levels of auxin are generally associated with faster growth. The resulting asymmetrical growth of cells elicits global curvature at the organism level through pathways that are not completely understood (54). Therefore, in our model auxin flux is a function of tropic signal and growth is taken to depend only on auxin concentration.

We assume that auxin is transported by diffusion and advection and locally removed by various mechanisms such as conjugation or direct oxidation (55–57). These effects are modeled through a standard reaction-advection-diffusion equation (58) for the auxin concentration $A(x_1, x_2, S, t)$:

$$\frac{\partial A}{\partial t} + \nabla \cdot \mathbf{J} = -QA + C, \qquad \mathbf{J} = -\kappa \nabla A + \mathbf{J}^{\text{stim}} \quad [4]$$

where $\mathbf{J}$ is the auxin flux, Q is a parameter that characterizes the rate of auxin turnover, and C captures any sources or sinks.

The flux is a sum of a *diffusive component* $\mathbf{J}^{\mathrm{diff}} = -\kappa\nabla A$, and a *stimulus component* $\mathbf{J}^{\mathrm{stim}}$, though a simple scaling analysis with estimated auxin diffusion and velocity (see SI Section 4A) suggests that the process is advection dominated, and so we restrict our attention to the zero diffusion limit $\kappa \to 0$. Depending on the particular tropism, the information about the stimuli is contained either in $\mathbf{J}^{\mathrm{stim}}$, or in a boundary or source term. The auxin transport equation Eq. (4) is combined with a no-flux condition $\mathbf{J}\cdot\mathbf{n} = 0$ at the outer boundary of each cross section, where $\mathbf{n}$ is an outward normal vector to the boundary $\partial\Omega_S$.

D. Tissue-level growth and remodeling. Once the auxin distribution is known from the solution of Eq. (4), we can relate the growth field at the tissue level to the concentration A. Here, we use the general theory of morphoelasticity (17) that assigns at each point of the plant a growth tensor dictating the deformation due to growth. Physically, this tensor field integrates the multiple contributions of local pressure, cell material properties and tissue geometry, all regulated via the cell metabolic and genetic activity into a single object describing the local change of shape of an elementary volume element (59). This growth tensor may be different in different directions (anisotropic growth) and/or spatially varying (heterogeneous growth) (60) to encode both changes in length and girth. However, here we will assume that growth only takes place, locally, along the axial direction and not in the cross-sectional direction. This assumption implies that there is no change in thickness, an effect that could be of importance in some systems. Then, the only non-trivial component of the growth tensor is a single function $g(x_1, x_2, S, t)$ that describes the change of axial length of an infinitesimal volume element (see SI Section 2). An initially straight filament of length L_0 with g constant at all points would grow to a new straight filament of length $L = L_0(1 + g(t))$ (18). If, however, $g = g(x_1, x_2, S, t)$ varies from point to point, the same filament would tend to bend and twist as shown in Fig. 2.

Next, we connect the axial growth function $g = g(x_1, x_2, S, t)$ to the concentration of auxin $A = A(x_1, x_2, S, t)$ via a growth law of the form

$$\frac{\partial g}{\partial t} = \beta(A - A^*) - \xi(g - \overline{g}), \qquad [5]$$

where A^* is a baseline level of auxin, β characterizes the rate at which an increase in auxin generates growth, and

$$\overline{g} = \frac{1}{\mathcal{A}}\int_{\Omega_S} g\,\mathrm{d}x_1\mathrm{d}x_2$$

is the average of the growth field. The term $\xi(g - \overline{g})$ provides a point-wise measure of the strain induced by differential growth and models *autotropism*, the observed tendency to grow straight when subject to other tropisms. The underlying mechanisms of autotropism are poorly understood but studies using radiolabeled auxin suggest that this straightening response does not depend on auxin but is sensed via an actomyosin-dependent mechanism (61, 62).

E. Change in local shape and properties. The axial growth function g is defined at the tissue scale and, as such, does not directly give the change in curvature and torsion of the plant. Indeed, the change of shape depends not only on g but also on the internal mechanical balance of the forces generated by each growing volume element. Following the general theory given in (18) and its adaptation to the particular case of plants given by the growth law Eq. (5), we compute the intrinsic curvatures and elongation of the growing plant (SI Section 3). In the absence of autotropism ($\xi = 0$), these curvatures (given by the vector $\hat{\mathbf{u}}$) define the shape of the plant in the absence of body force and external loads:

$$\mathcal{I}\frac{\partial \hat{\mathrm{u}}_1}{\partial t} = \beta\int_{\Omega_S} x_2 A\,\mathrm{d}x_1\mathrm{d}x_2, \qquad [6]$$

$$\mathcal{I}\frac{\partial \hat{\mathrm{u}}_2}{\partial t} = -\beta\int_{\Omega_S} x_1 A\,\mathrm{d}x_1\mathrm{d}x_2, \qquad [7]$$

$$\frac{\partial \hat{\mathrm{u}}_3}{\partial t} = 0, \qquad [8]$$

$$\mathcal{A}\frac{\partial \gamma}{\partial t} = \beta\int_{\Omega_S} (A - A^*)\,\mathrm{d}x_1\mathrm{d}x_2. \qquad [9]$$

Here and for the rest of the paper, we have assumed that the cross section is circular with radius R, area $\mathcal{A} = \pi R^2/2$ and second moment of area $\mathcal{I} = \pi R^4/4$.

F. Rod mechanics sets the plant position in the stimulus field. Once the intrinsic curvatures and elongation of the plant following growth have been updated, the plant position and orientation are updated by solving the Kirchhoff equations (41, 63) for the balance of linear and angular momentum for given external forces such as self-weight, wind, or contact forces (see SI Section 1 for details on the Kirchhoff equations).

Since at this scale the plant is treated as a one-dimensional structure, its equilibrium shape is easily computed even in complex non-planar geometries. Once the deformation is determined, the multiscale cycle is completed by updating the map between external stimulus and cell-scale response with respect to the updated orientation, and the process is repeated.

G. Summary. The flow of information between different spatial scales for a given stimulus field proceeds as follows:

(I) given an initial plant shape, a stimulus $\mathbf{F}$ impacts auxin transport and thus local concentrations of auxin via the transport equation (4);

(II) the local auxin concentration A changes the local growth field that impacts the intrinsic curvatures and axial extension of the plant via Eqs. (6)–(9);

(III) the new intrinsic curvatures and external conditions determine the new mechanical equilibrium of the plant, thus changing the plant position and shape in the stimulus field.

The theoretical objective in this work is to bridge the divide between cell-based descriptions of auxin transport and plant-level descriptions of tropism kinematics. In the examples below, we demonstrate how the tissue-level transport and growth equations may be mathematically combined to yield explicit evolution rules for the curvature and axial growth at the rod level. In this way, the multiscale flow can be efficiently simulated and analyzed for a variety of tropic responses. Though it is also worth noting that a significant amount of biology exists between the cell-scale and the tissue-level models we propose, therefore we largely opt for qualitative investigation of complex behavior, with further experimental and theoretical work needed to refine parameter selection.

2. Examples

A. Gravitropism. Gravitropism has been extensively studied both experimentally and theoretically. The classic description is based on the so-called the 'sine rule' in which the change in curvature follows the sine of the angle with the direction of gravity (64). While it is successful in capturing observed behavior in gravitropic experiments, it is mostly phenomenological and is only applicable to planar geometry. Here, we show that the sine rule emerges naturally from our formulation but that it can be generalized to include three-dimensional deformations that are generated when the entire plant is forced to change its orientation in time.

The stimulus for gravitropism is the vector field $\mathbf{F} = -G\mathbf{e}_3$ which can be written in the plant frame of reference as $\mathbf{F} = \mathbf{f} + \mathsf{f}_3\mathbf{d}_3$ where $\mathbf{f} := \mathsf{f}_1\mathbf{d}_1 + \mathsf{f}_2\mathbf{d}_2$ is the gravity force acting in the plane of the cross section. Since it is believed that plants are insensitive to the strength of gravitational field (65), it is sufficient to use a unit vector representing only the direction of gravity, i.e. we scale the gravitational acceleration G to 1. If $\mathbf{f} \equiv \mathbf{0}$, no tropic response will occur. Gravity perception relies on specific cells called *statocytes* distributed along the shoot (66). Statocytes contain dense organelles, *statoliths*, that sediment under the effect of gravity. Tilting of the plant causes statoliths to avalanche and to form a free surface perpendicular to the gravity vector, providing orientational information to the cell (67). It has been observed that the gravitropic response depends upon the angle between the statoliths free surface and the vertical, but not upon the intensity of the gravitational field or the pressure of statoliths against the cell membrane (65). A possible mechanism is that the contact between the statoliths and the cell membrane may trigger relocalization of PIN membrane transporters and a redirection of auxin flux (67). Here, we follow this hypothesis and, accordingly, assume that gravity drives an advective flow of auxin $\mathbf{J}^{\text{stim}} = kA\mathbf{f}$. If the statocytes are uniformly distributed within the stem volume then k is constant. We assume also a source and sink of auxin on each cross section, representing a continual axial auxin flow, and that auxin transport occurs on timescales much shorter than the one associated with growth. Combining the transport equation (Eq. (4)), growth law (Eq. (5)) (in the absence of autotropism for simplicity), and the evolution laws given by Eqs. (6)–(9), we obtain (see SI Section 4B) the *gravitropic curvature* and axial extension models:

$$\frac{\partial \hat{\mathsf{u}}_1}{\partial t} = \mathcal{C}_{\text{grav}}\mathsf{f}_2, \quad \frac{\partial \hat{\mathsf{u}}_2}{\partial t} = -\mathcal{C}_{\text{grav}}\mathsf{f}_1, \tag{10}$$

$$\frac{\partial \gamma}{\partial t} = \beta\left(\frac{\Delta C}{Q\mathcal{A}} - A^*\right). \tag{11}$$

Here, $\mathcal{C}_{\text{grav}} = \beta k \Delta C/(\mathcal{I}Q^2)$ is a single constant characterizing the rate of change of curvature due to gravity and associated with a timescale of gravitropic reaction $t_{\text{grav}} = 1/\left(L\mathcal{C}_{\text{grav}}\right)$, where L is a characteristic axial length, say the length of the plant, Q characterizes the constant rate of auxin turnover (Eq. (4)), and the parameter ΔC is the net auxin available in the cross section (see SI Section 4B). Note that the right-hand side of Eq. (11) is proportional to the net 'excess auxin', the integral of $(A - A^*)$ over the section, while the quantity A^* does not appear in Eq. (10). The existence of such an auxin threshold is observed both in local biosynthesis and developmental processes (68, 69) and adopted in models (e.g. (70)). In our model curvature may develop without axial extension: for axial extension the net auxin must exceed a threshold, while curvature development conceptually derives from a redistribution and thus asymmetry of auxin.

In the particular case where the plant can only bend around the single axis $\mathbf{d}_2$ and all external forces can be neglected, we have $\mathsf{f}_2 \equiv 0$, $\hat{\mathsf{u}}_1 \equiv 0$ and the curvature $\mathsf{u} = \hat{\mathsf{u}}_2$. Defining α to be the inclination angle, Eq. (10) reads

$$\frac{\partial \mathsf{u}}{\partial t} = -\mathcal{C}_{\text{grav}} \sin\alpha, \tag{12}$$

which is the classic and widely-used sine law of gravitropism (24).

The general evolution equations (Eqs. (10) and (11)) can be used for more complex gravitropic scenarios. Consider, for instance, an experiment in which the base of the plant stem is at a fixed angle θ from the horizontal and the base is rotated, as shown in Fig. 4(A) and used in experiments to study gravitational setpoint angles (71). Then, in the frame of reference of the plant, the direction of gravity is constantly changing. Here, we consider the case of zero-axial growth and neglect self-weight (see Section C for these additional effects). The tropic response will generate curvature and torsion depending on the angle and the rotational velocity of the base as shown in Fig. 4.

For visualization purposes, we fix the base rotation rate to one turn per unit time and vary the tropic reaction rate of the plant, which is equivalent to a fixed reaction rate and varying base rotation rate via a rescaling of time. In Fig. 4, we simulate three full rotations of the base with varying reaction rates (see also SI movies 1-4). The evolving morphology is characterized by three metrics: an alignment metric in (B) that measures how closely aligned with the vertical the plant is (a value of one is attained if the entire plant is vertical), and curvature and torsion in (C) that broadly measure deviation from a straight configuration (details in SI Section 5).

Consider first the slowest reaction morphology (equivalent to the case of fastest base rotation), given by the black curves in Fig. 4(B)-(C). Since the plant's response time is much slower than the base rotation, the gravitropic response is averaged out and the plant hardly deviates from the straight configuration, never improving its alignment and generating effectively no curvature or torsion. The plant is almost perfectly straight at all times (snapshots not included). The red curves denote a case with increased but still small reaction (fast base), which generates only small oscillations in alignment and curvature. In this regime, the plant is effectively 'confused'; the local gravitational field is changing too quickly for the plant to make any progress towards alignment with the gravitational field.

As the reaction rate is increased (or the base rotation decreased), interesting morphologies emerge. In the case of the intermediate reaction rate $\mathcal{C}_{\text{grav}} = 10$ (green curves), the plant begins to curve towards the vertical during the first quarter rotation of the base, bending about the $\mathbf{d}_2$ axis and increasing its alignment. However, as the base continues to rotate, the curvature initially developed has the tip pointing away from the vertical, so the alignment decreases, and the plant now must bend about the orthogonal $\mathbf{d}_1$ axis. As the

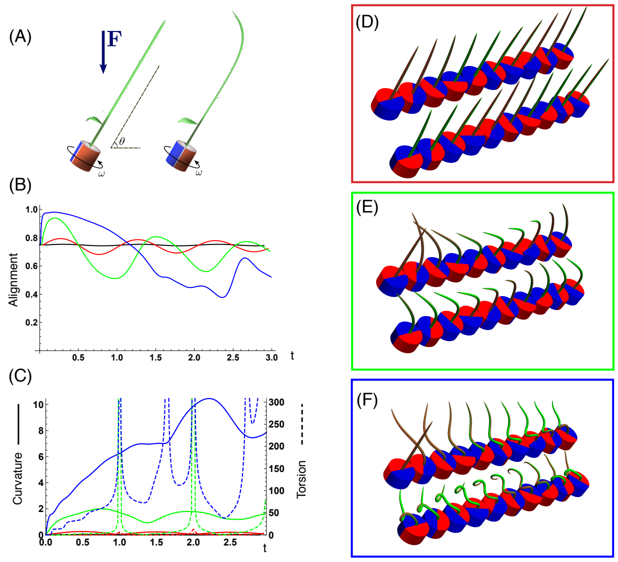

Fig. 4. Gravitropism with a rotating base. (A) A base is tilted with respect to the vertical and then rotated about the axis with speed so that one revolution is completed every time unit. Gravitropic response is simulated for varying values of gravitropic sensitivity $\mathcal{C}_{\text{grav}} = 0.1$ (black), 1 (red), 10 (green), and 50 (blue). Alignment with the vertical (B) and curvature and torsion (C) are plotted against time for three base rotations. Snapshots for cases of (D) slow reaction, $\mathcal{C}_{\text{grav}} = 1$, (E) intermediate reaction, $\mathcal{C}_{\text{grav}} = 10$, and (F) fast reaction, $\mathcal{C}_{\text{grav}} = 50$. The sequence is read left to right, top to bottom, and the base rotation is counterclockwise. Further simulation details and parameters provided in SI Section 8.

base completes its first rotation and the 'desired' axis for bending returns to the original $\mathbf{d}_2$, an inversion occurs (more visible in the movies provided in SI), creating a large spike in torsion that remains bounded and continuous. This basic process repeats with each rotation.

Finally, increasing the reaction rate (or slowing the base) further creates highly complex morphologies as evidenced by the blue curves. Here the plant quickly aligns with gravity and attains near perfect alignment in the first tenth of the first rotation. As the base rotates away from this aligned state, we see an interesting phenomenon: the tip of the plant is able to react and maintain alignment with the vertical, but since the base of the plant is clamped at an ever-changing angle, a loop forms starting at the base and working its way to the tip. This is accompanied by strong variations in the total alignment and increasingly high curvature, with repeated spikes in torsion as extra twist is removed. Our simulations of this case beyond three rotations suggest that while the basic process of loops generated at the base and working to the tip continues, the morphology does not settle down into a fixed oscillatory pattern, highlighting the potential for complex dynamics generated by this highly nonlinear system.

B. Phototropism. It was Darwin, at the end of the 19th Century, who demonstrated that exposure of the plant apex to a light source was necessary to induce tropic bending (5, 72). Later on, Boysen-Jensen proposed that bending is induced by a diffusive substance, later identified as auxin, that carries the tropic information from the apex to the rest of the shoot (73, 74). These early observations are the basis of the popular Cholodny-Went model (75, 76) stating that phototropism relies upon three broad mechanisms: *(i)* sensing of light direction at the tip of the shoot; *(ii)* establishment of a lateral asymmetry of auxin concentration at the tip; and *(iii)* basipetal transport of this asymmetrical distribution, resulting in differential growth along the shoot (77–79).

We model these three steps by considering *axial* transport of auxin, with an asymmetrical distribution that is established at the shoot apex by the stimulus, treated as a point source of light. We suppose that auxin flows basipetally with advective velocity U and turnover Q, for which the transport equation is

$$\frac{\partial A}{\partial t} - \frac{\partial}{\partial s}\left(UA\right) = -QA. \qquad [13]$$

Here the derivative in space is taken with respect to the current arc length $s \in [0, \ell]$. Additional source/sink terms can be used to model axial extension without changing the evolution of the curvature but are omitted in the first instance. We account for the amount and distribution of auxin at each section via a boundary condition at the tip ($s = \ell$) and define $A_{\text{tip}}(x_1, x_2, t) = A(x_1, x_2, \ell, t)$ that depends on the light source located at $\mathbf{p}(t)$ in space, and a scalar $I(t)$ representing its intensity. We then define the unit vector e from the plant tip to the light source and write it in the plant reference frame: $\mathsf{e}(t) = \mathsf{e}_1\mathbf{d}_1(\ell) + \mathsf{e}_2\mathbf{d}_2(\ell) + \mathsf{e}_3\mathbf{d}_3(\ell)$, as shown in Fig. 3(C). The vector $\mathsf{e}_1\mathbf{d}_1 + \mathsf{e}_2\mathbf{d}_2$ in the cross section distinguishes the light side of the tip from the dark side and defines the asymmetrical distribution of auxin:

$$A_{\text{tip}}(x_1, x_2, t) = -\kappa I(t)\left(\mathsf{e}_1(t)x_1 + \mathsf{e}_2(t)x_2\right), \qquad [14]$$

where κ characterizes the sensitivity of the phototropic response.

For constant velocity U, and in the absence of autotropic effects, Eqs. (13) and (14) can be solved exactly (SI Section 4C), which gives the *phototropic curvature model*:

$$\frac{\partial \hat{\mathrm{u}}_1}{\partial t} = -\mathcal{C}_{\text{photo}} \exp\left(\frac{-Q(\ell - s)}{U}\right) \mathsf{e}_2\left(t - \frac{\ell - s}{U}\right) \qquad [15]$$

$$\frac{\partial \hat{\mathrm{u}}_2}{\partial t} = \mathcal{C}_{\text{photo}} \exp\left(\frac{-Q(\ell - s)}{U}\right) \mathsf{e}_1\left(t - \frac{\ell - s}{U}\right), \qquad [16]$$

where $\mathcal{C}_{\text{photo}} := \beta\kappa I$ is a single parameter from which the phototropic response time is defined as $t_{\text{photo}} := 1/\left(L\mathcal{C}_{\text{photo}}\right)$. The exponential decay in Eq. (15) is due to the turnover of auxin so that less is available at the base, while the time shift $t_{\text{tran}} := L/U$ of A_{tip} accounts for the transport time to the section at arc length s, leading to time-delay differential equations. The change of curvature thus depends on three quantities: *(i)* the orientation of the tip with respect to the light source $t = (\ell - s)/U$ ago; *(ii)* the amount of auxin available for the phototropic signal, which depends on the turnover Q; and *(iii)* the plant's response sensitivity, characterized by $\mathcal{C}_{\text{photo}}$. Bending occurs over a characteristic dimensionless bending length $\ell_{\text{bend}} := U/(Q\ell)$ within the tip of the plant.

B.1. Fixed light source–no growth. We consider first a fixed light source and restrict our attention to the case of zero axial growth so that $\ell = L$ for all time and the transport equation is solved in the reference variables. For a given transport time t_{tran}, the response of the plant is determined by the characteristic dimensionless bending length ℓ_{bend} and the response time as shown in Fig. 5. With small bending length, the response is localized close to the tip, and the plant is much slower to orient (comparing (A) and (B)). Increasing the response

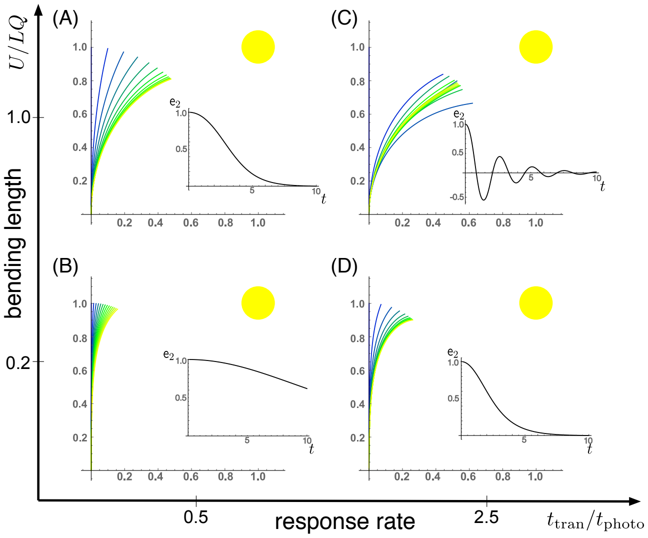

Fig. 5. Planar phototropic shape evolution for a fixed light source and with no axial growth, for small and large values of the ratio of response rate to transport rate $t_{\text{tran}}/t_{\text{photo}}$ and dimensionless bending length $\ell_{\text{bend}} = U/(QL)$. Inset: alignment is characterized by $\mathsf{e}_2(t)$, such that $\mathsf{e}_2 = 0$ when the tip is pointed at the source for this planar case. Further simulation details and parameters provided in SI Section 8.

rate naturally produces a faster orientation and potentially an overshoot. If axial auxin transport is much faster than the growth response ($t_{\text{tran}} \ll t_{\text{photo}}$), then the auxin is effectively in steady state at each growth step (as we have assumed for the cross-sectional transport). This implies that the delay can be neglected and the curvature response at each point depends on the *current* orientation of the tip. In this case, since the response is characterized entirely by the orientation of a single point, the motion is very simple: the plant bends to orient with the light, with no oscillations about the state in which the tip is perfectly oriented with the light ($\mathsf{e}_2 = 0$).

Contrast this behavior with gravitropism, in which an oscillation about the vertical state is typical unless a strong autotropism response is added. The difference between the gravitropic model and the phototropic model for fast transport is that during gravitropism, each cross section tries to align *itself* with gravity, thus creating a conflict at the global level that results in an oscillatory motion; while during phototropism each cross section tries to align the tip with the light, so there is no conflict. However, with delay, such a conflict does exist, due to the fact that each cross section is accessing a previous state of the tip. Thus, in the regime $t_{\text{tran}} \sim t_{\text{photo}}$, and if the bending length is not too short, a damped oscillation about the preferred orientation is observed, as shown in Fig. 5(C).

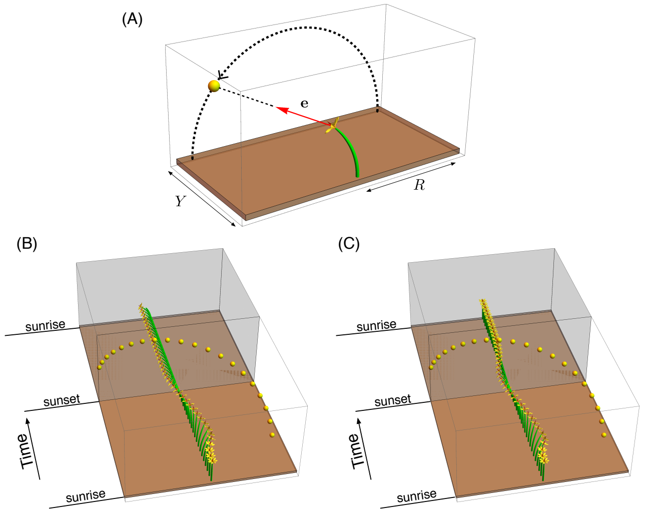

Fig. 6. (A) Geometry of the phototropic response stimulated by a light source that follows a circular path of radius R, shifted a distance Y in the transverse 'horizon'. (B) A full day-night cycle with fast response and long bending length. (C) the addition of autotropic terms enables the plant to return to the vertical during night, when the phototropic signal is absent. Further simulation details and parameters provided in SI Section 8.

B.2. Moving light source. Next, we consider a moving source, and in particular we simulate a day-night cycle of a plant following a light source (the sun) as shown in Fig. 6(A). The intensity $I(t)$ is also taken to be sinusoidal, so that the phototropic signal is strongest at noon and the signal vanishes at sunset. For fast response and long bending length, the plant bends significantly and successfully tracks the moving light source (Fig. 6(B)). However, at night and without a signal, the motion halts (see also SI movie 5). The plant remains bent towards sunset the entire night and does not display the nocturnal reorientation observed in many plants (80, 81). With a non-vanishing autotropic term ξ in Eq. (5), we obtain an *autophototropism curvature model* of the form:

$$\frac{\partial \hat{\mathsf{u}}_1}{\partial t} = -\mathcal{C}_{\text{photo}} \exp\left(\frac{-Q(\ell - s)}{U}\right) \mathsf{e}_2\left(t - \frac{\ell - s}{U}\right) - \xi \hat{\mathsf{u}}_1, \quad [17]$$

$$\frac{\partial \hat{\mathsf{u}}_2}{\partial t} = \mathcal{C}_{\text{photo}} \exp\left(\frac{-Q(\ell - s)}{U}\right) \mathsf{e}_1\left(t - \frac{\ell - s}{U}\right) - \xi \hat{\mathsf{u}}_2. \quad [18]$$

The additional terms serve to straighten the plant in the absence of any other signal. This is evident in Fig. 6(C), in which we see that the motion during the day is very similar,

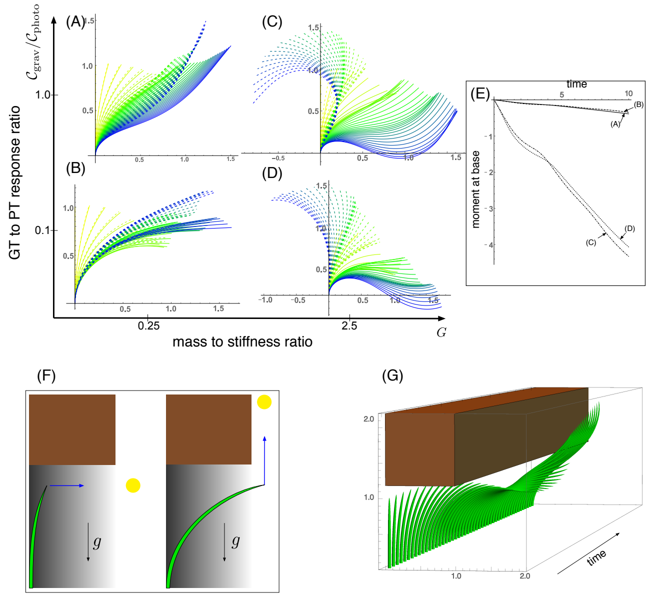

Fig. 7. Gravitropism versus phototropism. In (A)-(E), a fixed light source is located to the right, at the point (4,1), while gravity points vertically downward. For each parameter set, the tropic response is simulated for the same total time and with equivalent axial growth. The evolving plant shape, deformed under self-weight, is shown in increasing time from yellow to blue, with the unstressed shape appearing as a dashed line. The moment at the base for the 4 cases is plotted against time in (E). (F) depicts the setup for a plant escaping from the shade under a rigid obstacle. The phototropic signal either points horizontally, if the tip is under the shade, or vertically, if the tip is out of the shaded region. (G) a sample simulation showing a successful escape. Further simulation details and parameters provided in SI Section 8.

while at night the stem straightens back to the vertical (see also SI movie 6). We note that in heliotropic plants such as the common sunflower, *Helianthus annuus*, there are additional mechanisms, not considered here, based on circadian rhythms to reorient the plant at night to face eastward in anticipation of the next sunrise (82).

C. Photogravitropic response. Next, we demonstrate the delicate balance that must exist in the presence of tropic responses to multiple stimuli. We simulate two different scenarios of a plant responding to simultaneous but conflicting gravitropic and phototropic signals. Following (12), we assume that the effects of multiple stimuli are additive (see SI Section 4F). This assumption is based on the existence of separate pathways for signal transduction leading to the redistribution of auxin. However, it is known that these pathways share common molecular processes and there are non-trivial interactions between different tropisms (83) that will not be included here.

C.1. Fixed horizontal light source. We consider a growing plant subject to self-weight and initially oriented vertically, but with a fixed light source located in the transverse horizontal direction. The evolution of the plant can then be characterized by the ratio of response rates to gravitropic versus phototropic signals, and the ratio of density to bending stiffness, which controls the degree of deformation under self-weight.

In Fig. 7(A)-(D) we show the evolving morphology of the plant in this two-dimensional parameter space, plotting both the deformed shape (solid lines) and the reference unstressed shape (dashed lines). In (A), (B), the effect of self-weight is relatively minimal, and the evolution is primarily driven by the conflicting phototropic signal acting horizontally to the right, and the vertical gravitropic signal. With increased mass, there is an increased mechanical deformation due to self-weight, so that significant disparity develops between the deformed and reference shapes. In this regime the balance of signals has greater importance for the fate of the plant. Comparing (B) and (D), the initial phases are similar, but as the plant lengthens and extends to the right in (D), self-weight deforms the plant significantly, with half of the plant below the base level by the end of the simulation. Such a deformation could signal failure by creating large torque at the base. In (E) we plot the moment at the base, where the stress is highest, against time for each case, and as expected the moment is significantly higher for larger mass.

Intuitively, we expect that this problem could be alleviated by increasing the gravitropic response rate. Comparing (C) and (D), the evolution with higher gravitropic response in (C) does show decreased sagging. However, the moment at the base is in fact higher in (C). Increasing the gravitropic response rate even further does ultimately alleviate the problem – consider that the plant remains mostly vertical if gravitropism dominates phototropism – nevertheless, this example highlights the delicate and potentially counterintuitive nature of this balance.

C.2. Escaping from the shade. The results above suggest a view of a plant as a problem-solving agent that actively responds to the signals in its environment. A typical problem that many plants have to solve is access to light (84). For instance, consider a plant growing underneath a canopy (85) as shown in Fig. 7(F) and (G). While the tip is in the shaded region, diffuse lighting creates a phototropic stimulus to grow horizontally, orthogonal to the gravitational signal. If the tip emerges from under the shade, phototropism and gravitropism align, and the plant will attempt to grow vertically. In this mixed signal scenario, the success or failure of the plant in emerging from under the canopy is down to how the competing signals are integrated, and the relative importance of self-weight. An example of a successful escape is shown in Fig. 7(G). Note that determining the mechanical forces acting in the plant is crucial in this example: once the tip is outside of the shade, both signals try to align the entire length of the plant with the vertical, and this leads to physical contact between the plant and the corner of the canopy. Determining the morphology beyond this point thus requires determining the mechanical contact force (see SI Section 6) that would not be possible in a purely kinematic description.

D. Pole dancing. A fascinating plant motion is the mesmerizing dance that climbing plants, such as twiners, perform to first find a pole and then wrap around it. Like any dance, this event requires a complex integration of stimuli to achieve a well-orchestrated sequence of steps: *(i)* finding a pole, *(ii)* contacting the pole, and *(iii)* proceeding to wrap around the pole. A common mechanism for searching for a climbing frame is circumnutation, a combination of circular movement and axial growth causing the tip to move up in a sweeping spiral path, as first described by Darwin (5, 26, 86). When the plant makes contact with a pole, it must then interpret its orientation with respect to the pole in order to wrap around it. Here the stimulus is mechanical: the physical contact of the plant with the pole results in a change of curvature, a response referred to as thigmotropism. Since initially the plant only samples a very small region of the pole, the stimulus field is highly localized. As the plant wraps around the pole, new contact points are established to propagate the helical shape upward.

D.1. Circumnutation. Experiments suggest that, depending on the plant, circumnutation is either driven by an internal oscillator, a time-delay response to gravity, or a combination of the two (87, 88). Here, following the hypothesis of an internal oscillator, we show that the basic nutating motion emerges naturally from an internal oscillator at a single point combined with axial auxin transport (89). We consider an auxin source at the point $s = s_c$ from which an auxin differential is transported axially. The auxin transport equation may be solved in a similar manner as in the phototropism case with an added rotational component in the local frame of the cross section due to an internal oscillator (Fig 3(D)). Taking for simplicity a constant rotation rate ω, we obtain (details in SI Section 4D) the *circumnutation curvature model*:

$$\frac{\partial \hat{\mathsf{u}}_1}{\partial t} = \mathcal{C}_{\text{circ}} \sin\left(\omega\left(t - \frac{|s-s_c|}{U}\right)\right) e^{-\frac{Q}{U}|s-s_c|}, \qquad [19]$$

$$\frac{\partial \hat{\mathsf{u}}_2}{\partial t} = -\mathcal{C}_{\text{circ}} \cos\left(\omega\left(t - \frac{|s-s_c|}{U}\right)\right) e^{-\frac{Q}{U}|s-s_c|}. \qquad [20]$$

Since the signal here is internal, there is no feedback from the environment and the morphology of the plant is predetermined by the turnover Q, the transport velocity U, the response rate $\mathcal{C}_{\text{circ}}$, and the rotation rate ω. In Fig. 8(A) we illustrate a sample motion with auxin source at the tip. Fig. 8(B) demonstrates the impact of auxin turnover: high turnover means the motion is constrained to a region very close to the tip and thus the elliptical shape of the tip pattern is small. More complex tip patterns may also be generated if there is non-uniformity in the internal oscillator (Fig. 8(C)).

D.2. Thigmotropism. Two interesting observations can be made when a twining plant makes first contact with a pole: *(i)* torsion is generated via a localized contact around a single point, and *(ii)* a rotation is induced, i.e. the orientation of the tangent of the plant with respect to the axis of the pole changes. These observations suggest that this contact is sufficient to generate locally a helical shape, and that the pitch of the helix is fixed by internal parameters as opposed to the angle at which contact is made (90, 91).

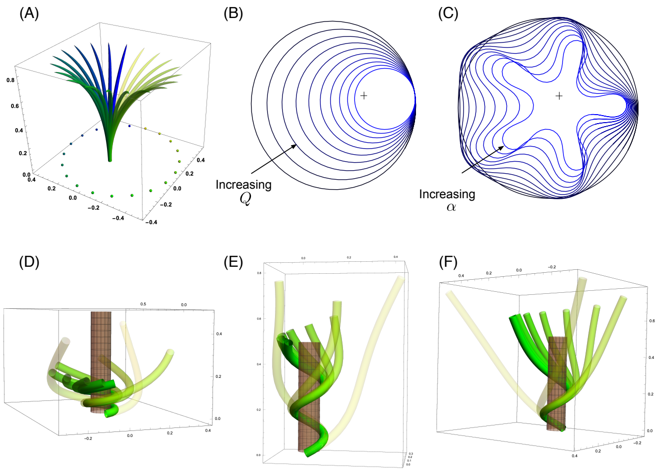

Fig. 8. Circumnutation (A)-(C) and thigmotropism (D)-(F). (A) snapshots of a sample circumnutation motion, with tip pattern projected onto the plane. In (B) and (C), tip patterns are plotted for varying parameters (the location of the plant base is indicated by the cross). In (B), an increase in turnover Q decreases the size of the tip pattern. In (C), a non-constant angular velocity of the oscillator is given by $\omega = \hat{\omega} + \alpha\cos(5t)$, generating a tip pattern with 5-fold symmetry, and increasingly non-circular with increasing α. In (D)-(F), the wrapping around a pole due to thigmotropism via a single contact point is simulated for the same total time, for different parameter regimes: with low rotational component (D), the torsion is low, a high rotational component with low turnover (E) generates rapid wrapping and high torsion, while wrapping is much slower with high turnover (F). Further simulation details and parameters provided in SI Section 8.

To show how pole wrapping can be obtained within our framework consistently with these observations, we consider a plant with a single contact point located at $s = 0$, and at position on the boundary Ω_0 with angle ψ_0 in the plane $\mathbf{d}_1$-$\mathbf{d}_2$. The contact induces an auxin gradient at this point, with maximal auxin on the opposite side of the contact point, i.e. $A(0, x_1, x_2) = -F(\cos\psi_0\, x_1 + \sin\psi_0\, x_2)$, and the auxin is transported by an advective flux with both an axial component U and a constant rotational component with angular velocity ω (Fig 3(E)). The transport equation can be solved exactly (SI Section 4E), and we obtain the following *thigmotropism curvature model*:

$$\frac{\partial \hat{\mathsf{u}}_1}{\partial t} = -\mathcal{C}_{\text{thig}} \exp\left(-\frac{Qs}{U}\right) \sin\left(\psi_0 + \frac{\omega s}{U}\right), \qquad [21]$$

$$\frac{\partial \hat{\mathsf{u}}_2}{\partial t} = \mathcal{C}_{\text{thig}} \exp\left(-\frac{Qs}{U}\right) \cos\left(\psi_0 + \frac{\omega s}{U}\right). \qquad [22]$$

Solving these equations leads to exact expressions for the intrinsic curvatures from which we extract the geometric curvature $\kappa = \mathcal{C}_{\text{thig}} \exp\left(-Qs/U\right) t$ and torsion $\tau = \omega/U$ (see SI Section 8F). The curvature increases linearly in time until it reaches a maximal value determined by the pole radius (the intrinsic curvature may keep increasing, but the actual curvature may not due to the mechanical contact). For a pole of radius c and plant radius a the helix radius $\alpha = c + a$ is fixed, while the helical angle ϕ depends on the rotation rate and is found to satisfy $\sin(2\phi) = \omega\alpha/U$.

For given axial velocity U, the resulting helical shape is determined solely by the geometry of the pole and the rotational component ω, while the wrapping rate depends on the turnover Q and the response rate $\mathcal{C}_{\text{thig}}$. In Fig. 8(D)-(F) we illustrate three different regimes: low rotational component with low turnover (D), high rotational component with low turnover (E), and high rotational component with high turnover (F) (see also SI movies 7-9). Note that at time $\hat{\kappa}/\mathcal{C}_{\text{thig}}$ where $\hat{\kappa}$ is the final curvature, the contact point spreads to a contact region, creating a wave of contact and auxin signal that propagates along the length of the plant. Here, we restrict our attention to the signal from the first contact point. The separate curvature models for circumnutation and pole wrapping can now be combined to simulate the process of searching for a pole, making contact, and wrapping (see SI movie 10).

3. Model validation

The tropic scenarios we have considered thus far were not focused on specific plants or experiments, but rather with the aim of demonstrating a diverse range of complex behavior. To validate the framework as a general construct, in Fig. 9 we compare model output with data in three distinct experimental scenarios that together include all of the tropisms we have modeled: (A) includes data on thigmotropic curvature generation (92) and gravitropic bending, (B) shows a diversity of tip patterns measured during circumnutation (93), and (C) plots the evolving shape of saplings bending to align with gravity and exposed to isotropic (left) or anisotropic (right) light (94) (see SI Section 9 for details of these experiments and model comparison). In each case, the model is able to reproduce, qualitatively and quantitatively, the experimental observations, demonstrating a robustness of the framework across a range of plant types and combined tropic responses.

A second type of validation is obtained by considering the simplification of our models to existing purely kinematic models. A number of geometric models exist in the literature, positing the evolution of the plant's curvature as a function of time, and have been systematically validated against data and observations. The sine law (Eq. (12)) is an example of such a kinematic model. Similarly, planar kinematic phototropic (12) and circumnutation models (95) have been proposed and we show explicitly in SI Section 7 that they can be reproduced from the models we have derived under particular geometric restrictions and/or parameter limits. Our framework both generalizes these descriptions and enables potential insight to how changes at the level of auxin transport and tissue growth might be seen in organ-level kinematics.

4. Conclusion

Plant motion in response to environmental stimuli is a process of extreme biological and ecological relevance. While the pioneering biologists of the 19th Century investigated the global motion of plants via clever experiments devised to create conflicting signals and generate complex plant morphologies, most of the work of the 20th Century was focused on the molecular and cellular processes, seeking signaling pathways and relevant proteins involved in tropic response. We have combined this accumulated knowledge with recent progress in the physical and computational modeling of living structures to develop a general framework for tropism that relates stimuli to shape. To do so, we modeled auxin transport and the mechanisms by which environmental stimuli are integrated into cellular activities, tissue-level growth, leading ultimately to a change in shape at the plant scale viewed as a morphoelastic structure.

We have demonstrated the power of this framework through a series of examples including key effects such as axial growth, autotropism, gravitropism, phototropism, thigmotropism, self-weight, circumnutation, contact mechanics, and three-dimensional deformations. The specific tropic scenarios we have considered were chosen to illustrate the range of complex behaviors capable of being simulated. The study of individual stimuli provided new models for the evolution of curvatures for different form of tropisms. These models can be confronted, and refined, iteratively, against data and experiments as needed. Further, we demonstrated the potential for multiple

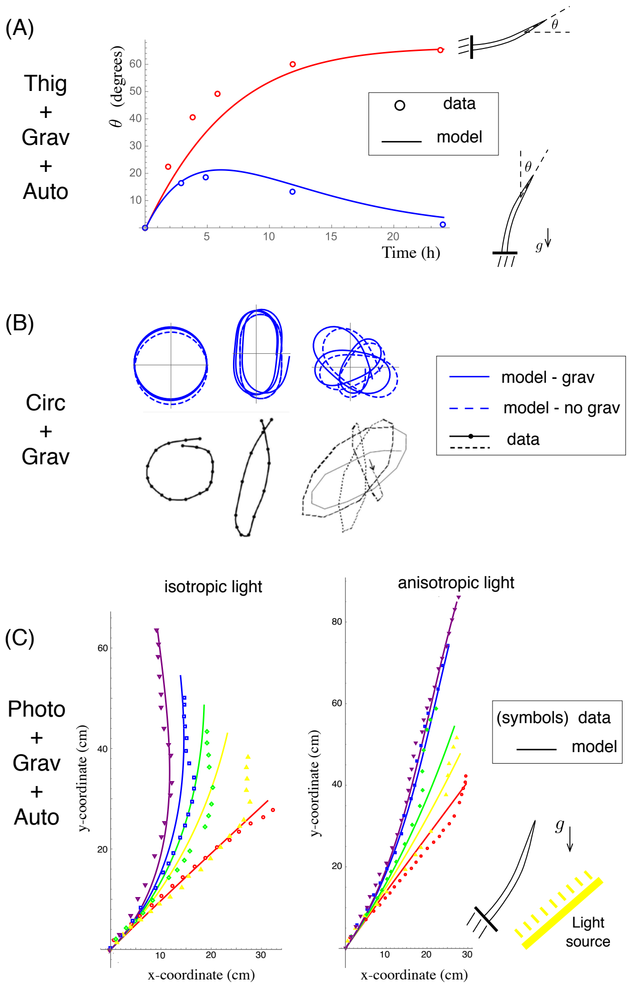

Fig. 9. A comparison of model output with experimental observations for a variety of tropic responses. (A) Mechanical perturbation is applied to cucumber hypocotyls situated vertically, causing them to bend (blue data and curves), after which they recover the vertical; a horizontally-situated plant bends toward the vertical under gravitropism (red data and curves). (B) Multiple tip patterns are observed in sunflowers; these circumnutation patterns are reproduced by the model with (solid curves) and without (dashed curves) gravitropic effects. (C) Tree saplings are inclined at an angle and subjected to either isotropic (left) or anisotropic (right) light. The shape of the plants is extracted at 5 times and discretized along the length (symbols). Continuous 2D shapes (solid curves) obtained by our model combining gravitropic, phototropic, and autotropic effects are included at the same time points.

and potentially conflicting stimuli to create *problems* for the plant to *solve*. The resulting plant behaviors indicate a need for a delicate balance between competing tropisms to achieve a particular task. In each particular scenario, we have opted for parsimony over complexity in terms of modeling choices, in order to highlight qualitative features and how auxin-level differences may become apparent in plant-level morphology.

The work presented here integrated information at the tissue and organ levels. This approach needs to be expanded to include cell-based and molecular-level descriptions to fully link the scales for tropisms and plant growth. At the cell to tissue scale, the link between auxin and growth in Eq. (5) is a lumped description of a complex process that involves cell wall tension and turgor pressure (96). In principle, additional modeling layers could also be added between the stimulus and auxin response, including for example transcription factors and protein production and interactions. Both of these extensions likely require explicit cell-based modeling. However, our framework is such that if the output from a cell model is the value of the piecewise continuous axial growth function g, then the evolution of the curvatures given by Eqs. (6)–(8) still applies and can be used to infer the global changes of geometry. Another important extension is to include branching processes since most of these filamentary structures include multiple branches. Branches can easily be included within a rod theory, at the additional cost of including extra parameters, such as length and orientation of each segments, and new growth laws for the placement of each segment (28, 32).

This work provides a theoretical platform for understanding plant tropisms and generating complex morphologies. As well as linking to cellular and subcellular scales, a key future direction is connecting with experiments dedicated to controlling multiple stimuli and generating complex morphologies. For instance, we showed that a relatively simple experimental set-up like a rotating base under gravity can generate a wide range of plant shapes. Such steps espouse an approach that is both multiscale and multidisciplinary. Indeed, plants refuse to obey by the rules of a single scientific discipline. They are not simply genetic or cellular entities, nor are they purely physical objects or ecological atoms. They reach for the sun, they bend under gravity, they feel their neighbors, they grow, twist, curve, and dance in the fresh air and in the dark caves. If we have any hope to understand them, we will need to respect their plurality, break down our own disciplinary barriers, and fully integrate our scientific knowledge from subcellular to ecological levels.

ACKNOWLEDGMENTS. The support for A.G. by the Engineering and Physical Sciences Research Council of Great Britain under research grant EP/R020205/1 is gratefully acknowledged. The authors thank János Karsai for permission to use his flower parameterisation in Fig. 6.

1. Firn RD, Digby J (1980) The establishment of tropic curvatures in plants. *Annual Review of Plant Physiology* 31(1):131–148.
2. Band LR, et al. (2012) Root gravitropism is regulated by a transient lateral auxin gradient controlled by a tipping-point mechanism. *Proceedings of the National Academy of Sciences* 109(12):4668–4673.
3. Bastien R, Bohr T, Moulia B, Douady S (2013) Unifying model of shoot gravitropism reveals proprioception as a central feature of posture control in plants. *PNAS* 110(2):755–760.
4. Simmons C, Söll D, Migliaccio F (1995) Circumnutation and gravitropism cause root waving in arabidopsis thaliana. *Journal of Experimental Botany* 46(1):143–150.
5. Darwin C (1897) *The power of movement in plants.* (Appleton).
6. Sachs J (1888) *Lectures on the Physiology of Plants, English Edn. Warehouse.* (Oxford University Press).
7. Moulia B, Fournier M (2009) The power and control of gravitropic movements in plants: a biomechanical and systems biology view. *Journal of experimental botany* 60(2):461–486.
8. Vos J, et al. (2009) Functional–structural plant modelling: a new versatile tool in crop science. *Journal of experimental botany* 61(8):2101–2115.
9. Esmon C, Pedmale U, Liscum E (2005) Plant tropisms: providing the power of movement to a sessile organism. *The International Journal of Developmental Biology* 49(5-6):665–674.
10. Sato E, Hijazi H, Bennett M, Vissenberg K, Swarup R (2014) New insights into root gravitropic signalling. *J exp botany* 66(8):2155–2165.
11. Mattheck CM, Mattheck C (1998) *Design in nature: learning from trees.* (Springer Science & Business Media).
12. Bastien R, Douady S, Moulia B (2015) A unified model of shoot tropism in plants: photo-, gravi-and propio-ception. *PLoS Comput Biol* 11(2):e1004037.
13. Pfeffer WFP (1904) *Pflanzenphysiologie: ein Handbuch der Lehre vom Stoffwechsels und Kraftwechsels in der Pflanze.* (W. Engelmann).
14. Bonnet C (1779) *Mémoires d'histoire naturelle. Recherches sur l'usage des feuilles.* (De l'imprimerie de Samuel Fauche, libraire du roi).
15. Duhamel du Monceau HL (1758) La physique des arbres (the physics of trees). l. guérin et l. *F. Delatour, Paris, France.*
16. Whippo CW, Hangarter RP (2006) Phototropism: bending towards enlightenment. *The Plant Cell* 18(5):1110–1119.
17. Goriely A (2017) *The mathematics and mechanics of biological growth.* (Springer).
18. Moulton DE, Lessinnes T, Goriely A (2020) Morphoelastic rods III: Differential growth and curvature generation in elastic filaments. *Journal of the Mechanics and Physics of Solids* 142:104022.
19. Tabor M, Klapper I (1996) Dynamics of twist and writhe and the modeling of bacterial fibers in *Mathematical Approaches to Biomolecular Structure and Dynamics.* (Springer), pp. 139–159.
20. Klapper I (1996) Biological applications of the dynamics of twisted elastic rods. *Journal of Computational Physics* 125(2):325–337.
21. Schlick T (1995) Modeling superhelical DNA: recent analytical and dynamic approaches. *Current Opinion in Structural Biology* 5(2):245–262.
22. Thompson JMT, van der Heijden GHM, Neukirch S (2002) Supercoiling of DNA plasmids: mechanics of the generalized ply. *Proceedings of the Royal Society of London. Series A: Mathematical, Physical and Engineering Sciences* 458(2020):959–985.
23. Muthert LWF, Izzo LG, Van Zanten M, Aronne G (2019) Root tropisms: Investigations on earth and in space to unravel plant growth direction. *Frontiers in Plant Science* 10.
24. Bastien R, Douady S, Moulia B (2014) A unifying modeling of plant shoot gravitropism with an explicit account of the effects of growth. *Frontiers in Plant Science* 5.
25. Meroz Y, Porat A, Tedone F, Palladino M, Marcati P (2020) A general 3d model for growth dynamics of sensory-growth systems: from plants to robotics. *Frontiers in Robotics and AI* 7:89.
26. Goriely A, Neukirch S (2006) Mechanics of climbing and attachment in twining plants. *Phys. Rev. Lett.* 97(18):184302.
27. Chelakkot R, Mahadevan L (2017) On the growth and form of shoots. *J Roy Soc Interface* 14(128):20170001.
28. Faruk Senan N, O'Reilly O, Tresierras T (2008) Modeling the growth and branching of plants: a simple rod-based model. *J Mech Phys Sol* 56(10):3021–3036.
29. Guillon T, Dumont Y, Fourcaud T (2012) A new mathematical framework for modelling the biomechanics of growing trees with rod theory. *Mathematical and Computer Modelling* 55(9):2061–2077.
30. O'Reilly OM, Tresierras TN (2011) On the evolution of intrinsic curvature in rod-based models of growth in long slender plant stems. *Int J Solids and Structures* 48(9):1239–1247.
31. O'Reilly OM (2017) *Modeling Nonlinear Problems in the Mechanics of Strings and Rods.* (Springer).
32. Jirasek C, Prusinkiewicz P, Moulia B (2000) Integrating biomechanics into developmental plant models expressed using l-systems. *Plant biomechanics* pp. 615–624.
33. Evers J, van der Krol A, Vos J, Struik P (2011) Understanding shoot branching by modelling form and function. *Trends in plant science* 16(9):464–467.
34. Surovy P, Yoshimoto A (2013) Application of a Functional-Structural Plant Model (FSPM) to Optimize a Management Regime. *FORMATH* 12:173–189.
35. Fozard J, Bennett M, King J, Jensen O (2016) Hybrid vertex-midline modelling of elongated plant organs. *Interface Focus* 6(5):20160043–14.
36. Jensen OE, Fozard JA (2015) Multiscale Models in the Biomechanics of Plant Growth. *Physiology* 30(2):159–166.
37. Antman SS (2005) *Nonlinear problems of elasticity.* (Springer New York).
38. Pai DK (2002) Strands: Interactive simulation of thin solids using cosserat models in *Computer Graphics Forum.* (Wiley Online Library), Vol. 21, pp. 347–352.
39. Manning RS, Maddocks JH, Kahn JD (1996) A continuum rod model of sequence-dependent DNA structure. *J. Chem. Phys.* 105:5626–5646.
40. Chouaieb N, Goriely A, Maddocks JH (2006) Helices. *Proc. Natl. Acad. Sci. USA* 103(25):9398–9403.
41. Moulton DE, Lessinnes T, Goriely A (2012) Morphoelastic rods Part 1: A single growing elastic rod. *Journal of the Mechanics and Physics of Solids* 61(2):398–427.
42. Carmo MPD (1976) *Differential geometry of curves and surfaces.* (Prentice-Hall, New Jersey).
43. Bishop RL (1975) There is more than one way to frame a curve. *Amer. Math. Month.* 82.
44. Braybrook SA, Peaucelle A (2013) Mechano-Chemical Aspects of Organ Formation in Arabidopsis thaliana: The Relationship between Auxin and Pectin. *PloS one* 8(3):e57813.
45. Lockhart JA (1965) An analysis of irreversible plant cell elongation. *Journal of Theoretical Biology* 8(2):264–275.
46. Cosgrove DJ (2005) Growth of the plant cell wall. *Nature Reviews Molecular Cell Biology* 6(11):850–861.
47. Boudon F, et al. (2015) A Computational Framework for 3D Mechanical Modeling of Plant Morphogenesis with Cellular Resolution. *PLoS Computational Biology* 11(1).
48. Bassel GW, et al. (2014) Mechanical constraints imposed by 3D cellular geometry and arrangement modulate growth patterns in the Arabidopsis embryo. *PNAS* 111(23):8685–8690.
49. Daher FB, et al. (2018) Anisotropic growth is achieved through the additive mechanical effect

of material anisotropy and elastic asymmetry. *eLife* 7.

50. Kennaway R, Coen E, Green A, Bangham A (2011) Generation of diverse biological forms through combinatorial interactions between tissue polarity and growth. *PLoS Computational Biology* 7(6):e1002071.
51. Muday GK (2001) Auxins and tropisms. *Journal of plant growth regulation* 20(3):226–243.
52. Gilroy S (2008) Plant tropisms.
53. Esmon CA, et al. (2006) A gradient of auxin and auxin-dependent transcription precedes tropic growth responses. *Proceedings of the National Academy of Sciences* 103(1):236–241.
54. Vanneste S, Friml J (2009) Auxin: a trigger for change in plant development. *Cell* 136(6):1005–1016.
55. Rose S, Rubery PH, Bopp M (1983) The mechanism of auxin uptake and accumulation in moss protonemata. *Physiologia Plantarum* 58(1):52–56.
56. Woodward AW, Bartel B (2005) Auxin: regulation, action, and interaction. *Annals of botany* 95(5):707–735.
57. Benková E, et al. (2003) Local, efflux-dependent auxin gradients as a common module for plant organ formation. *Cell* 115(5):591–602.
58. Runions A, Smith RS, Prusinkiewicz P (2014) Computational models of auxin-driven development in *Auxin and Its Role in Plant Development.* (Springer-Verlag Wien), pp. 315–357.
59. Rodriguez EK, Hoger A, McCulloch AD (1994) Stress-dependent finite growth in soft elastic tissues. *Journal of biomechanics* 27(4):455–467.
60. Coen E, Rolland-Lagan AG, Matthews M, Bangham JA, Prusinkiewicz P (2004) The genetics of geometry. *Proceedings of the National Academy of Sciences of the United States of America* 101(14):4728–4735.
61. Okamoto K, et al. (2015) Regulation of organ straightening and plant posture by an actin–myosin xi cytoskeleton. *Nature plants* 1(4):1–7.
62. Harmer SL, Brooks CJ (2018) Growth-mediated plant movements: hidden in plain sight. *Current opinion in plant biology* 41:89–94.
63. Nizette M, Goriely A (1999) Towards a classification of euler–kirchhoff filaments. *Journal of mathematical physics* 40(6):2830–2866.
64. Galland P (2002) Tropisms of avena coleoptiles: sine law for gravitropism, exponential law for photogravitropic equilibrium. *Planta* 215(5):779–784.
65. Chauvet H, Pouliquen O, Forterre Y, Legué V, Moulia B (2016) Inclination not force is sensed by plants during shoot gravitropism. *Scientific Reports* 6.
66. Morita MT (2010) Directional gravity sensing in gravitropism. *Annual review of plant biology* 61:705–720.
67. Pouliquen O, et al. (2017) A new scenario for gravity detection in plants: the position sensor hypothesis. *Physical Biology* 14(3):035005.
68. Mousdale D, Fidgeon C, Wilson G (1985) Auxin content and growth patterns in auxin-dependent and auxin-autotrophic plant cell and tissue cultures. *Biologia plantarum* 27(4-5):257.
69. Chandler JW (2009) Local auxin production: a small contribution to a big field. *Bioessays* 31(1):60–70.
70. Bozorg B, Krupinski P, Jönsson H (2016) A continuous growth model for plant tissue. *Physical Biology* 13(6):65002.
71. Roychoudhry S, Del Bianco M, Kieffer M, Kepinski S (2013) Auxin Controls Gravitropic Setpoint Angle in Higher Plant Lateral Branches. *Current Biology* 23(15):1497–1504.
72. Whippo CW, Hangarter RP (2006) Phototropism: Bending towards enlightenment.
73. Jensen PB (1911) La transmission de l'irritation phototropique dans l'avena. *Bulletin de l'Académie des Sciences et Lettres de Montpellier*.
74. Christie JM, Murphy AS (2013) Shoot phototropism in higher plants: New light through old concepts. *American Journal of Botany* 100(1):35–46.
75. Cholodny N (1927) Wuchshormone and tropismen bei den pflanzen. *Biol Zentralbl* 47:604–629.
76. Went FW (1928) Wuchsstoff und wachstum. *Rec Trav Bot Neerl* 25:1–116.
77. Went FW, Thimann KV, , et al. (1937) Phytohormones. *Phytohormones.*
78. Hart JW (1992) *Plant tropisms and other growth movements.* (Chapman & Hall), p. 208.
79. Christie JM (2007) Phototropin blue-light receptors. *Annu. Rev. Plant Biol.* 58:21–45.
80. Stanton ML, Galen C (1993) Blue light controls solar tracking by flowers of an alpine plant. *Plant, Cell & Environment* 16(8):983–989.
81. Vandenbrink JP, Brown EA, Harmer SL, Blackman BK (2014) Turning heads: the biology of solar tracking in sunflower. *Plant Science* 224:20–26.
82. Atamian HS, et al. (2016) Circadian regulation of sunflower heliotropism, floral orientation, and pollinator visits. *Science* 353(6299):587–590.
83. Correll MJ, Kiss JZ (2002) Interactions between gravitropism and phototropism in plants. *Journal of plant growth regulation* 21(2):89–101.
84. Ballaré CL, Pierik R (2017) The shade-avoidance syndrome: Multiple signals and ecological consequences. *Plant, cell & environment* 40(11):2530–2543.
85. Ballaré C, Scopel A, Roush M, Radosevich S (1995) How plants find light in patchy canopies. a comparison between wild-type and phytochrome-b-deficient mutant plants of cucumber. *Functional Ecology* pp. 859–868.
86. Isnard S, Silk WK (2009) Moving with climbing plants from charles darwin's time into the 21st century. *American Journal of Botany* 96(7):1205–1221.
87. Brown AH (1993) Circumnutations: From Darwin to space flights.
88. Agostinelli D, DeSimone A, Noselli G (2020) Nutations in plant shoots: endogenous and exogenous factors in the presence of mechanical deformations. *bioRxiv.*
89. Stolarz M (2009) Circumnutation as a visible plant action and reaction: physiological, cellular and molecular basis for circumnutations. *Plant signaling & behavior* 4(5):380–387.
90. Silk WK (1989) On the curving and twining of stems. *Environmental and Experimental Botany* 29(1):95–109.
91. Silk WK (1989) Growth rate patterns which maintain a helical tissue tube. *Journal of theoretical Biology* 138(3):311–328.
92. Jaffe MJ, Takahashi H (1990) Thigmotropism and the inodulation of tropistic curvature by mechanical perturbation in cucumber hypocotyls. *Physiologia Plantarum* 80:561–567.
93. Stolarz M (2014) Circumnutation as a visible plant action and reaction. *Plant Signaling & Behavior* 4(5):380–387.
94. Coutand C, Adam B, Ploquin S, Moulia B (2019) A method for the quantification of phototropic and gravitropic sensitivities of plants combining an original experimental device with model-assisted phenotyping: Exploratory test of the method on three hardwood tree species. *PloS one* 14(1):e0209973–28.
95. Bastien R, Meroz Y (2016) The Kinematics of Plant Nutation Reveals a Simple Relation between Curvature and the Orientation of Differential Growth. *PLoS Computational Biology* 12(12):e1005238–20.
96. Mirabet V, Das P, Boudaoud A, Hamant O (2011) The role of mechanical forces in plant morphogenesis. *Annual review of plant biology* 62:365–385.